

Observed vertical structure of tropical oceanic clouds sorted in large-scale regimes

Hui Su,¹ Jonathan H. Jiang,¹ Deborah G. Vane,¹ and Graeme L. Stephens²

Received 3 September 2008; revised 28 October 2008; accepted 4 November 2008; published 27 December 2008.

[1] The CloudSat cloud water content (CWC) profiles are sorted by a number of large-scale parameters obtained from reanalysis and satellite observations, including 500 hPa vertical velocity, sea surface temperature and its gradient, surface divergence, precipitation, water vapor path, convective available potential energy and lower tropospheric static stability. The sorting is physics-based and phenomenon-oriented. We find different degrees of clustering of cloud vertical structure in various large-scale regimes. The dominant modes are the deep and shallow clouds with peak CWC above 7 km and below 2 km, respectively, corresponding to distinctly different large-scale regimes. A middle-level peak of CWC around 5–7 km is discernible associated with the large-scale conditions similar to the shallow clouds. This study provides the first quantitative and comprehensive view of tropical CWC distributions in large-scale regimes. These results offer insights into cloud parameterizations and serve as new observational metrics for evaluation of cloud simulations in models. **Citation:** Su, H., J. H. Jiang, D. G. Vane, and G. L. Stephens (2008), Observed vertical structure of tropical oceanic clouds sorted in large-scale regimes, *Geophys. Res. Lett.*, 35, L24704, doi:10.1029/2008GL035888.

1. Introduction

[2] Tropical cloud structure is closely related to the ambient large-scale dynamic and thermodynamic conditions. Emanuel [1994] showed that the transition of shallow clouds into deep clouds is associated with the warming of sea surface temperature (SST) and the change of large-scale descending regime into ascending regime. However, this general picture of cloud structure as a function of large-scale regimes needs observational quantification for cloud parameterizations and evaluation of cloud simulations in large-scale models. CloudSat, for the first time, makes this quantification possible by providing a global survey of cloud profiles from space-borne millimeter cloud profiling radar (CPR) since June 2006.

[3] Haynes and Stephens [2007] analyzed CloudSat cloud mask profiles in relation to precipitation. They found three cloud modes (deep, shallow and middle-level clouds) in the tropics, in line with the trimodal structure of tropical convection found by Johnson *et al.* [1999]. It has also been shown that different geographical regions exhibit different

characteristics of cloud vertical structure, in association with different dynamics [e.g., Kubar and Hartmann, 2008].

[4] An increasingly popular method to identify the relations of clouds with large-scale dynamics is to sort cloud profiles (and cloud radiative effects) by 500 hPa vertical velocity (ω_{500}). This sorting technique is proved to be useful in understanding cloud variability and identifying differences among models for cloud feedback estimates [e.g., Bony *et al.*, 2004; Wyant *et al.*, 2006]. Zhang *et al.* [2007] performed the “cluster analysis” on the vertical profiles of CloudSat radar reflectivity and sorted the occurrence frequency of each cloud cluster by NCEP ω_{500} . They stressed that the dynamics sorting technique is important for model-data comparisons.

[5] In this paper, we analyze 1-year (January to December 2007) of cloud water content (CWC) profiles from the CloudSat Level 2B Cloud Water Content Radar-Only product (R. T. Austin *et al.*, Retrievals of ice cloud microphysical parameters using the CloudSat millimeter-wave radar and temperature, submitted to *Journal of Geophysical Research*, 2008) and sort them by a number of large-scale parameters. The CWC is the sum of cloud liquid water content (LWC) and ice water content (IWC), both of which are usually direct model output variables and inputs to radiation calculations. Hence, analysis of these two observed quantities provides a direct reference for evaluation of simulated cloud amount and associated cloud radiative effects. The large-scale parameters we use here include not only ω_{500} , but also SST, surface convergence, SST gradient, precipitation, column-integrated water vapor path (WVP), convective available potential energy (CAPE), and lower tropospheric stability (LTS, defined as the potential temperature difference between 700 hPa and surface, as by Klein and Hartmann [1993]). Except ω_{500} , all other parameters are obtained or derived from satellite observations. The choice of these parameters is based on the existing knowledge of their connection with convection; yet a quantitative view of the observed CWC distributions in each large-scale regime is not known. We present the results in terms of the annual averages for Year 2007. The seasonal and day-night differences are discussed.

2. Data and Methodology

[6] CloudSat is a member of the A-train satellite constellation, with equatorial crossing time around 1:30 am/pm. The CloudSat footprint is 1.7 km along track and 1.3 km cross track. The vertical resolution is 480 m, oversampled to 240 m. The IWC and LWC are retrieved from the 94 GHz radar reflectivity (Ze) measurements using empirical log-linear relations between Ze and IWC/LWC. The limitation of the retrieval is estimated at $Ze = -31$ dBz. Thus

¹Jet Propulsion Laboratory, California Institute of Technology, Pasadena, California, USA.

²Department of Atmospheric Science, Colorado State University, Fort Collins, Colorado, USA.

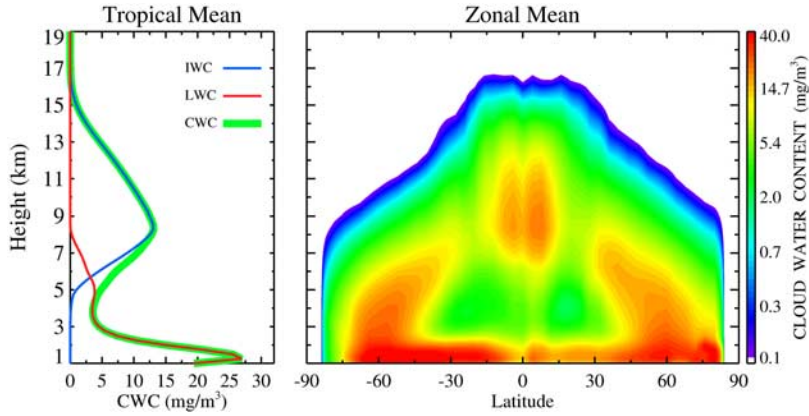


Figure 1. (a) Tropical and (b) zonal mean CWC (IWC+LWC) profiles observed by CloudSat averaged for 2007.

CloudSat cannot detect thin cirrus of small IWC and non-precipitation liquid clouds of small LWC. In precipitating clouds, CWC may be underestimated because the radar signal is dominated by precipitation and CWC retrieval is not possible. Moreover, due to the surface reflectance problem, CloudSat cannot see the clouds in the lowest kilometer near the surface. So we limit our analysis to cloud profiles above 0.5 km. Details about the IWC/LWC retrievals are described by Austin et al. (submitted manuscript, 2008).

[7] The collocation of large-scale parameters with the CloudSat measurements is greatly facilitated by the A-train. The Advanced Microwave Scanning Radiometer (AMSR-E) on Aqua provides nearly simultaneous SST and WVP measurements. We downloaded the twice-daily SST and WVP data with a resolution of $0.25^\circ \times 0.25^\circ$ from the Remote Sensing Systems (<http://www.remss.com>). SST gradient is then calculated using the centered difference scheme. The Atmospheric Infrared Sounder (AIRS) on Aqua provides atmospheric temperature and water vapor profiles. From its Level 3 product (with a horizontal resolution of $1^\circ \times 1^\circ$) we calculated CAPE and LTS twice a day. We assume an air parcel is lifted pseudo-adiabatically from 1000 hPa when calculating CAPE.

[8] Precipitation is from the Tropical Rainfall Measuring Mission (TRMM). We use the 3B42 3-hourly product with a resolution of $0.25^\circ \times 0.25^\circ$, which combines the rainfall estimates from radar, infrared and microwave instruments and rain gauges. We derive surface convergence using surface wind measurements from the Quick Scatterometer (QuikSCAT) and compare it with that calculated from the NCEP surface winds. The results are very similar as NCEP assimilates QuikSCAT winds in its analysis. As QuikSCAT orbits have large offsets from the CloudSat orbits in both time and space, we decided to use NCEP 6-hourly surface wind divergence instead of QuikSCAT to ensure maximum overlapping of CloudSat CWC with the surface divergence field. The ω_{500} is from NCEP, with a horizontal resolution of $2.5^\circ \times 2.5^\circ$.

[9] All large-scale variables are interpolated onto the CloudSat tracks in both space and time. For each large-scale variable, 25 bins are specified. Then the CWC profiles within each bin are averaged with clear-sky treated as zero CWC. Only tropical (30°S – 30°N) oceanic measure-

ments are considered in the binning. We used ~ 40 million cloud profiles for the one-year data analysis.

3. Geographical Distributions of Cloud Profiles

[10] Figure 1a shows the tropical-mean IWC, LWC and CWC profiles observed by CloudSat averaged for 2007 and Figure 1b shows the zonal mean CWC at all latitudes (clear-sky included as zero CWC). The tropical-mean CWC profile exhibits a double-peak structure: one at ~ 1.5 km and the other at ~ 8 km. The transition of liquid clouds into ice clouds occurs between 5 km to 8 km (the freezing layer) in the tropical-mean. The amplitude of IWC is much smaller than LWC. In the tropics, the strongest zonal-mean IWC is within 15° of the equator in the lower troposphere, with higher values in the northern hemisphere than in the southern hemisphere. Conversely, the maximum LWC is in the southern hemisphere subtropics. The maximum cloud top heights are over 16 km in the tropics and decrease poleward. In the mid-latitude storm tracks (45° – 75°S/N), CWC reaches maximum intensity below 2 km.

[11] Figure 2 shows the maps of annual mean CWC at four heights. Substantial differences exist at the four levels. At 2 km, large CWC (liquid only) occurs over the eastern Pacific (EP), the south Indian Ocean (IN), south Pacific convergence zone (SPCZ), inter-tropical convergence zone (ITCZ), northern South America (SAM), equatorial Atlantic (EA) and extra-tropical storm tracks. At 5 km, CWC (mostly LWC plus small amount of IWC) decreases markedly in EP, EA, ITCZ, SPCZ and extra-tropics; but it is stronger than or as strong as that at 2 km over western Pacific (WP), IN and SAM. CWC (IWC only) at 9 km is large in WP, South Asia, IN, SAM and central Africa, while it is more confined above these convective centers at 16 km and smaller in magnitude than that at 9 km by a factor of 20 or more.

4. Tropical Cloud Profiles Sorted by Large-Scale Parameters

[12] Figure 3 displays the one-year CWC profiles sorted by eight coincident large-scale parameters over the tropical oceans. The probability density functions (PDF) of each large-scale parameter are superimposed. We leave out the

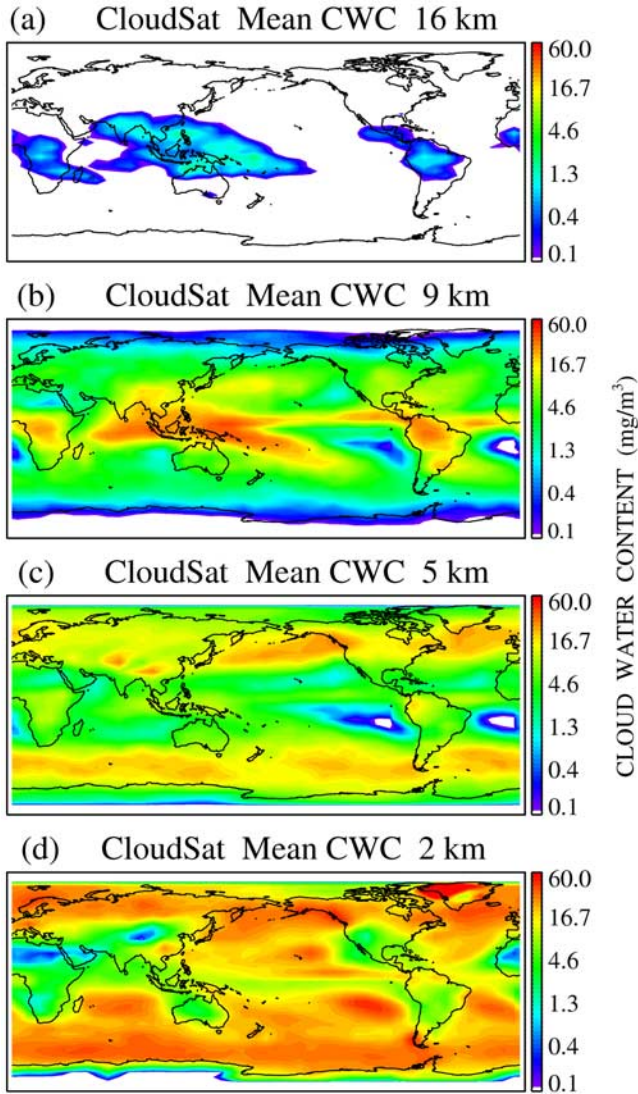


Figure 2. Maps of the annual mean CloudSat observed CWC at four heights: (a) 16 km, (b) 9 km, (c) 5 km and (d) 2 km.

bins within which the number of measurements is less than 150. We also tried a variant of the display of the bin plots in which stretched x-axes in proportion to the PDF of the large-scale variables were used as in *Wyant et al.* [2006]. The resulting CWC patterns highlight the dominant cloud modes but hide away the infrequent modes (figure not shown). To faithfully represent all possible observed cloud variabilities, we decided not to use the stretched x-axes. However, when comparing the observations with GCMs, using the stretched x-axes may be more useful. The horizontal maps of the annual-mean large-scale variables are also shown in Figure 3.

[13] To characterize the CWC distributions in each large-scale regime, we broadly categorize the cloud structure by the height of local CWC maxima: below 2 km as the shallow clouds, 5–7 km as the middle clouds and above 7 km as the deep clouds, in rough correspondence to *Johnson et al.* [1999] and *Haynes and Stephens* [2007]. Note that middle-level or deep convective clouds may bear

double peaks in the CWC vertical profiles, one in the boundary layer and one in the upper levels. In this case, the low-level peak is not regarded as a separate “shallow” mode. As illustrated in Figure 3, the actual CWC profiles for each mode exhibit large variabilities in different large-scale regimes.

4.1. 500 hPa Vertical Velocity (ω_{500})

[14] The PDF of ω_{500} is approximately symmetric about the peak near zero (shifted slightly positive), dictated by the tropical mass balance (Figure 3a). Ascents coincide with deep convective regions, while descents are in EP and the subtropics. In the large-scale ascent regime, the CWC profiles are “deep” with large CWC from 5 km to 15 km and a secondary peak (LWC) below 2 km. As ω_{500} changes from negative to positive, LWC increases. In the subsidence regime, clouds are “shallow” with maximum CWC in the boundary layer. Over the strongest subsidence regions ($\omega_{500} > 0.4$ Pa/s), cloud tops are capped below 3 km. The occurrence frequency of these clouds is about 6.3%. In Figure 3a, the middle-level clouds are not clear.

4.2. SST

[15] The horizontal map of SST shows close association with ω_{500} : large-scale ascents (descents) generally correspond to warm (cold) SST. However, the SST distribution is smoother than that of ω_{500} . Its PDF has a broad peak around 298–302 K. When sorted by SST, CWC exhibits three modes: the deep mode with peak CWC higher than 7 km in the warm SST (>300 K) regime, the shallow mode with maximum CWC below 2 km over the SST of ~288–300 K, and a weak middle-level mode with peak CWC around 5–7 km overlying the strong LWC in the boundary layer (Figure 3b). The CWC magnitude for the middle clouds is 10 times smaller than the deep and shallow clouds. Over the coldest SST (<290 K), the CWC profiles maximize in the high altitudes but the magnitudes are much weaker than the deep clouds over the warmer SST (>300 K). The occurrence frequency of these clouds is only 0.01%. They may result from the intrusion of mid-latitude storms into the subtropics or cirrus detrainments from convection over nearby land.

4.3. Surface Divergence

[16] Deep convection is usually associated with convergent flow near the surface. Figure 3c illustrates the cloud structure in the domain of surface divergence. The pattern of surface divergence resembles that of ω_{500} , with peak occurrence near zero (shifted towards 1×10^{-5} s⁻¹). The binned CWC shows the deep and shallow modes distinctly, and a weak but discernible middle mode. The deep mode is centered at surface convergence about -2×10^{-5} s⁻¹, with the high-level and low-level peaks of similar magnitudes. The shallow clouds are distributed over surface divergence from 0 to 2×10^{-5} s⁻¹. The weak middle-level mode is concentrated over surface divergence of 2×10^{-5} s⁻¹.

4.4. SST Gradient

[17] SST gradient is believed to be another important factor that determines tropical circulation and convection. In the tropics, the meridional SST gradient is much stronger than the zonal SST gradient and thus the magnitude of SST gradient shown in Figure 3h is dominated by the meridional

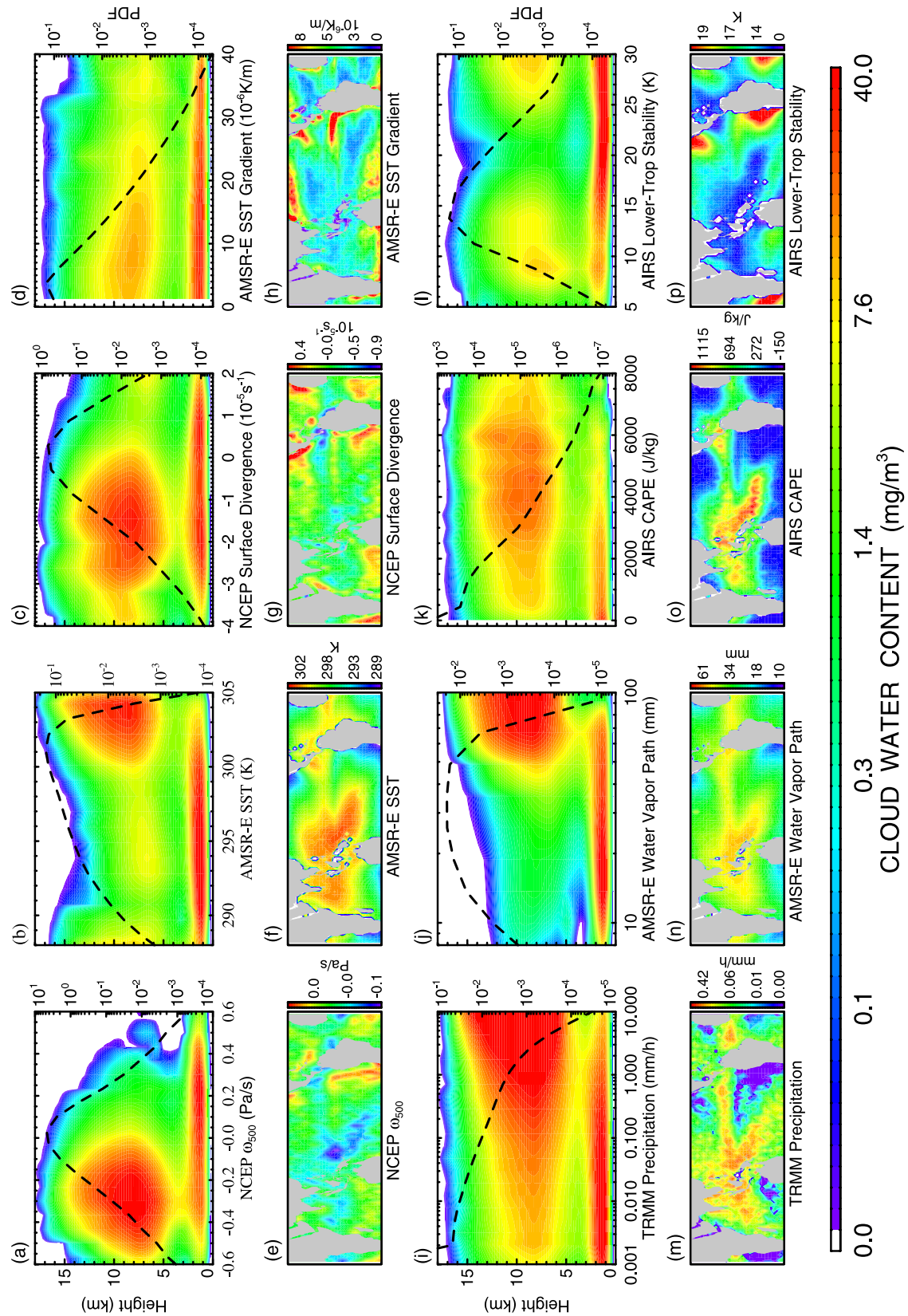


Figure 3. The CloudSat observed CWC profiles sorted by eight large-scale parameters. The PDF of each large-scale parameter is plotted in dashed black curve. The map of each large-scale parameter is shown below the corresponding binned plot.

SST gradient. Large SST gradients are observed in the equatorial EP, California and Peruvian coasts and subtropical oceans, mostly surface divergent regions. The PDF of SST gradient shows a nearly monotonic decrease as gradient increases. The binned CWC profiles are rather different from the previous three. Although the deep mode is evident over the relatively weak SST gradient regime, the peak CWC in the upper levels is much weaker than the counterparts in Figures 3a–3c. The high clouds are distributed quite evenly in the SST gradient domain, unlike the highly clustered structure in the domains of ω_{500} , SST and surface divergence. This suggests that the change of SST gradient only weakly affects the high cloud amount. The strongest CWC is distributed over the relatively weak SST gradient regime of 10×10^{-6} K/m, while the middle-level clouds are scattered over the large SST gradient between 30 and 40×10^{-6} K/m with very low occurrence frequency ($\sim 0.001\%$).

4.5. Precipitation

[18] Defining the minimum rain rate for precipitating clouds being 0.001 mm/h, we find that the occurrence frequency of precipitation over the tropical oceans is about 14.5% (If the threshold rain rate is raised to 0.1 mm/h, the tropical precipitation occurrence would be $\sim 7\%$, in closer agreement with Haynes and Stephens [2007]). About 85% of precipitating clouds have surface rain rates less than 2 mm/h and they contribute to 45% of tropical rainfall. Only 15% of the precipitating clouds have rain rates greater than 2 mm/h but they constitute about 55% of the total rainfall. Shallow clouds are spread over the weak precipitation regime, where the middle-level clouds are also pervasive. In the heavy precipitation regime (> 2 mm/h), the deep clouds dominate.

4.6. Water Vapor Path

[19] Atmospheric moisture is closely linked to cloud processes. The PDF of WVP has a broad peak from 20–50 mm and decreases sharply when WVP is greater than 50 mm. The moist air columns with WVP > 50 mm account for 0.3% of the total air columns, but they contain 57% of total precipitable water. Deep clouds are highly concentrated in the moist air columns and shallow clouds are distributed over the drier environment. Over the moistest regime, CWC peaks strongly in the upper levels with little liquid water below 5 km. There are hints of middle-level clouds in the drier air columns, but their CWC above 5 km is quite small.

4.7. Convective Available Potential Energy

[20] The CAPE is proportional to the buoyancy of an air parcel when it is lifted. Convection tends to consumes CAPE and restores atmosphere to neutral stability. Figure 3o shows the horizontal distribution of annual-mean CAPE for the tropical oceans. The pattern is very similar to that of precipitation and WVP, with the peak value around 1200 J/Kg over the deep convective regions. The instantaneous CAPE values are much higher. Its PDF is a monotonically decreasing function. The binned CWC profiles display certain degree of clustering: the shallow clouds occur over the low CAPE (< 500 J/Kg) regions and the deep clouds are associated with higher CAPE (> 4000 J/kg). The middle-level clouds seem to be indistinguishable from the deep clouds in

the CAPE domain as the CWC contours spread quite continuously between ~ 6 km and ~ 13 km.

4.8. Lower Tropospheric Stability

[21] The LTS is found highly correlated with the occurrence of stratiform clouds. The calculated LTS from AIRS is nearly a ‘complement’ to CAPE, in that high CAPE corresponds to low LTS and vice versa (Figure 3p). The PDF of LTS peaks around 14 K and skews to higher occurrence in large LTS than in small LTS. The shallow clouds are mostly distributed over stable lower troposphere with LTS > 14 K, while the double-peaked deep mode is concentrated over less stable lower troposphere where LTS is less than 10 K. In Figure 3i, a cluster of middle to high clouds are noticeable over very high LTS values (> 25 K), overlapping above strong LWC in the boundary layer. Their occurrence frequency is only 0.01%, though.

5. Seasonal and Day-Night Differences

[22] Besides the annual means, we also examined the seasonal and day-night differences for the regime-sorted cloud profiles. The overall characteristics of cloud clustering are consistent in all seasons (figure not shown). The major difference is the magnitudes of IWC and LWC. In general, the peak IWC for the deep clouds is larger in northern winter than in summer while the peak LWC for the stratiform clouds is larger in northern summer than in winter. Comparing the day-time (1:30pm) and night-time (1:30am) CWC, IWC tends to be larger in the day, while LWC tends to be larger at night due to more efficient radiative cooling at night than in the day.

6. Conclusions

[23] This study examines the CloudSat observed CWC profiles sorted in a number of large-scale regimes. We find that two distinct modes dominate the vertical structure of tropical clouds. The deep mode with the peak CWC around 8–10 km is associated with mid-tropospheric ascent, warm SST, surface convergence, weak SST gradient, heavy precipitation, moist air, large CAPE and weak lower-tropospheric static stability. The opposite conditions apply to the shallow clouds which have peak CWC (i.e., LWC) at 1–2 km. Although the deep and shallow modes are outstanding in all large-scale regimes, the actual CWC profiling for each mode varies in different large-scale parameter space. The linkage of the deep and shallow modes with their respective large-scale regimes is expected, but the quantification of the CWC amount in each regime is a significantly new result. We also find an infrequent middle-level cloud mode. These middle-level clouds usually have a peak CWC around 5–7 km and strong LWC in the boundary layer, under conditions that are not favorable to deep convection, i.e., cold SST, strong surface divergence, large SST gradient, dry air and stable lower troposphere. The hypothesis that these clouds may result from the influence of middle-latitude storms is largely ruled out when we find that the features for this mode are robust even when the binning averages are restricted to 15°S – 15°N , despite of their very low occurrence frequency (figures not shown). Therefore, we tend to think that these middle clouds may correspond to the

cumulus congestus that detrain near the freezing level as elaborated in *Johnson et al.* [1999]. The physical processes that produce these middle clouds need to be further studied. Exploring more large-scale parameters such as middle tropospheric humidity, lapse rate and wind shear as “regime-identifiers” may help to elucidate their origins. Given the limitations of CloudSat IWC/LWC retrievals (Austin et al., submitted manuscript, 2008), future work that combines CloudSat and CALIPSO measurements would provide a more complete representation of the tropical cloud structure.

[24] Although the association of cloud structure with large-scale dynamics has been established for a long time, the lack of observed CWC profiles in connection with large-scale regimes hindered the evaluation of cloud simulations and improvement of cloud parameterizations in climate models. The regime-sorted cloud profiles presented in this paper can serve as new observational metrics for comparison with models. Because they are physics-based and phenomenon-oriented, using them as model-data comparison metrics will likely better identify sources of model errors and point to the directions for model improvements. Next-generation model-data comparison should evolve beyond comparing the spatial and temporal means and make more use of these observational regime-specific cloud properties.

[25] **Acknowledgments.** We thank the JPL R&TD FY08 funding support, discussions with J. Teixeira and X. Huang, and helpful comments from the two reviewers. This work is conducted at the Jet Propulsion Laboratory, California Institute of Technology, under contract with NASA.

References

- Bony, S., et al. (2004), On dynamic and thermodynamic components of cloud changes, *Clim. Dyn.*, 22, 71–86.
- Emanuel, K. A. (1994), *Atmospheric Convection*, 580 pp., Oxford Univ. Press, Oxford, U. K.
- Haynes, J. M., and G. L. Stephens (2007), Tropical oceanic cloudiness and the incidence of precipitation, *Geophys. Res. Lett.*, 34, L09811, doi:10.1029/2007GL029335.
- Johnson, R. H., et al. (1999), Trimodal characteristics of tropical convection, *J. Clim.*, 12, 2397–2418.
- Klein, S. A., and D. L. Hartmann (1993), The seasonal cycle of low stratiform clouds, *J. Clim.*, 6, 1587–1606.
- Kubar, T. L., and D. L. Hartmann (2008), Vertical structure of tropical oceanic convective clouds and its relation to precipitation, *Geophys. Res. Lett.*, 35, L03804, doi:10.1029/2007GL032811.
- Wyant, M. C., et al. (2006), A comparison of low-latitude cloud properties and their response to climate change in three AGCMs sorted into regimes using mid-tropospheric vertical velocity, *Clim. Dyn.*, 27, 261–279.
- Zhang, Y., S. Klein, G. G. Mace, and J. Boyle (2007), Cluster analysis of tropical clouds using CloudSat data, *Geophys. Res. Lett.*, 34, L12813, doi:10.1029/2007GL029336.

J. H. Jiang, H. Su, and D. G. Vane, Jet Propulsion Laboratory, California Institute of Technology, Pasadena, CA 91109, USA. (hui.su@jpl.nasa.gov)
G. L. Stephens, Department of Atmospheric Science, Colorado State University, Fort Collins, CO 80523, USA.